https://doi.org/10.5194/egusphere-2024-2522
Preprint. Discussion started: 30 September 2024


# Locating and quantifying $CH_4$ sources within a wastewater treatment plant based on mobile measurements

Junyue Yang[1], Zhengning Xu[1], Zheng Xia[4,5], Xiangyu Pei[1], Yunye Yang[1], Botian Qiu[2,3], Shuang Zhao[2,3], Yuzhong Zhang[2,3*], Zhibin Wang[1,6*]

[1]Zhejiang Provincial Key Laboratory of Organic Pollution Process and Control, MOE Key Laboratory of Environment Remediation and Ecological Health, College of Environmental and Resource Sciences, Zhejiang University, Hangzhou 310058, China

[2]Key Laboratory of Coastal Environment and Resources of Zhejiang Province, School of Engineering, Westlake University, Hangzhou 310030, China

[3]Institute of Advanced Technology, Westlake Institute for Advanced Study, Hangzhou 310024, China

[4]Ecological and Environmental Monitoring Center of Zhejiang Province, Hangzhou 310012, China

[5]Zhejiang Key Laboratory of modern Ecological and Environmental Monitoring, Hangzhou 310012, China

[6]ZJU-Hangzhou Global Scientific and Technological Innovation Center, Zhejiang University, Hangzhou 311200, China

*Correspondence to*: Zhibin Wang (wangzhibin@zju.edu.cn) and Yuzhong Zhang (zhangyuzhong@westlake.edu.cn)

**Abstract.** Wastewater treatment plants (WWTPs) are substantial contributors to greenhouse gas (GHG) emission because of the high production of methane ($CH_4$) and nitrous oxide ($N_2O$). A typical WWTP complex contains multiple functional areas that are potential sources for GHG emissions. Accurately quantifying GHG emissions from

https://doi.org/10.5194/egusphere-2024-2522
Preprint. Discussion started: 30 September 2024


these sources is challenging due to the inaccuracy of emission data, the ambiguity of emission sources, and the absence of monitoring standards. Locating and quantifying WWTPs emission sources in combination with measurement-based GHG emission quantification methods are crucial for evaluating and improving traditional emission inventories. In this study, $CH_4$ mobile measurements were conducted within a WWTP complex in the summer and winter of 2023. We utilized a multi-source Gaussian plume model combined with the genetic algorithm inversion framework, designed to locate major sources within the plant and quantify the corresponding $CH_4$ emission fluxes. We identified 12 main point sources in the plant and estimated plant-scale $CH_4$ emission fluxes of 603.33 ± 152.66 t $a^{-1}$ for the summer and 418.95 ± 187.59 t $a^{-1}$ for the winter. The predominant sources of $CH_4$ emissions were the screen and primary clarifier, contributing 55 % and 67 % to the total emissions in summer and winter, respectively. The comparison against traditional emission inventories revealed that the $CH_4$ emission fluxes in the summer were 2.8 times greater than the inventory estimates, and in the winter, emissions were twice the inventory values. Our flux inversion method achieved a good agreement between simulations and observations (correlation > 0.6 and a root mean square error (RMSE) < 0.7 mg $m^{-3}$). This study demonstrated that mobile measurements, combined with the multi-source Gaussian plume inversion framework, are a powerful tool to locate and quantify GHG sources in a complex site, with the potential for further refinement to accommodate different types of factories and gas species.

## 1 Introduction

Greenhouse gas (GHG) emissions exacerbate the greenhouse effect, causing adverse impacts on human health, ecosystems, and the environment (IPCC, 2023). Methane ($CH_4$) is the second-largest contributor to climate change, with the global warming potential 27.9 times that of carbon dioxide ($CO_2$). Reducing $CH_4$ emissions is essential

https://doi.org/10.5194/egusphere-2024-2522
Preprint. Discussion started: 30 September 2024


for mitigating climate change and progressively achieving the global target of limiting warming to 1.5 °C. The latest observational study from the WMO Global Atmospheric Watch network indicated that the global annual average concentration of $CH_4$ in 2022 was 1923 ± 2 ppb, representing a 264 % increase from pre-industrial levels (WMO, 2023). The International Energy Agency (IEA) 's 2024 Global Methane Tracker report suggests that global $CH_4$ emissions reached 580 Mt in 2023, with anthropogenic $CH_4$ emissions accounting for 60 %. The complexity of $CH_4$ emission processes, lack of monitoring systems, and limitations of emission estimation models present challenges in accurately estimating anthropogenic $CH_4$ emissions.

The quantification of $CH_4$ emission fluxes is typically achieved through a bottom-up inventory method. However, due to the difficulties in obtaining actual emission factors activity data, and specific information on different emission sources, there is considerable uncertainty in the assessing of the emission inventory method (Lin et al., 2021). In contrast, a top-down method that estimates $CH_4$ emissions by monitoring atmospheric concentration has been increasingly applied in recent years (Sun et al., 2019; Cusworth et al., 2024; Han et al., 2024; Maazallahi et al., 2023; Riddick et al., 2017). The monitoring technology mainly includes satellite (Zhang et al., 2021; Liang et al., 2023; Jacob et al., 2022) and airborne (Allen et al., 2019; Abeywickrama et al., 2023; Cui et al., 2017) remote sensing, as well as ground-based monitoring such as vehicle-based mobile monitoring (Albertson et al., 2016; Al-Shalan et al., 2022; Caulton et al., 2018), station monitoring (Dietrich et al., 2021; Hase et al., 2015; Heerah et al.,2021) and tower monitoring (Richardson et al., 2017; Balashov et al., 2020). Numerous studies use satellite remote sensing, unmanned aerial vehicle (UAV) monitoring, and vehicle-based mobile monitoring techniques to measure $CH_4$ emissions (Sun et al.,2023). However, satellite spatiotemporal resolution is limited and UAVs have short endurance, making vehicle-based mobile monitoring a better choice for measuring emissions at wastewater treatment plants (WWTPs). Vehicle-based mobile monitoring can perform continuous real-time monitoring and precise identification of

https://doi.org/10.5194/egusphere-2024-2522
Preprint. Discussion started: 30 September 2024


emission sources, and hence have been applied to urban (von Fischer et al., 2017; Defratyka et al., 2021) and plant-scale (Zhao et al., 2021; Jin et al.,2010) monitoring of GHG concentrations and emission fluxes. Vogel et al. (2024) investigated $CH_4$ leaks in 12 cities across 8 countries, using high-precision fast-response GHG analyzers combined with the mobile survey methodology (von Fischer et al., 2017). Chen et al. (2020) utilized the multiple-Gaussian-plume model and a forward modeling approach for mobile measurements of $CH_4$ emissions during the Munich Oktoberfest. Shi et al. (2023) proposed a $CO_2$/$CH_4$ emission quantification model (EMISSION-PARTITION) and conducted mobile measurements with vehicle-based monitoring system at chemical, coal washing, and waste incineration plants in two cities and one industrial park in China, assuming different numbers of emission sources for quantitative assessment. Wang et al. (2022a; 2022b) employed the Environmental Protection Agency's Other Test Method 33A (OTM 33A) for monitoring downwind of fueling stations to estimate the $CH_4$ emission fluxes of nine compressed natural gas (CNG) stations and five liquefied natural gas (LNG) stations in Eastern China. Emission flux inversion methods also include isotope tracer method (Jackson et al., 2014; Zimnoch et al., 2018), cross-sectional flux method (Luther et al., 2019; Makarova et al., 2021), and atmospheric diffusion model inversion method (Kumar et al., 2021; Yacovitch et al., 2015). Atmospheric transport models with varied degrees of complexity, including Gaussian diffusion models (Stadler et al., 2021), Lagrangian models (Mckain et al., 2015), and Eulerian models (Bergamaschi et al., 2018), are used in the inversion to relate GHG concentrations with emissions. Optimization methods, such as Bayesian optimization (Karion et al., 2019) and linear regression models (Kumar et al., 2021), are applied to achieve accurate inversion results. Furthermore, some studies incorporate carbon isotope observations to better attribute the contribution of different $CH_4$ emission sources (Maazallahi et al., 2020).

As a significant source of GHG emissions, WWTPs generate substantial amounts of $CH_4$, $N_2O$, and $CO_2$ during the collection, treatment, and discharge of sewage and

https://doi.org/10.5194/egusphere-2024-2522
Preprint. Discussion started: 30 September 2024


sludge, contributing 3 % of the global total GHG emissions (Bai et al., 2022). The estimation of $CH_4$ emission fluxes from WWTPs has increasingly attracted widespread attention. Li et al. (2024) developed a plant-level and technology-based $CH_4$ emission inventory for municipal WWTPs in China, estimating the $CH_4$ emissions for 2020 to be 150.6 Gg. Wang et al. (2022) systematically considered process technological differences in wastewater treatment, constructing a high-resolution greenhouse gas emission inventory for Chinese WWTPs from 2006 to 2019. Delre et al. (2017) measured the $CH_4$ and $N_2O$ concentrations downwind of five WWTPs in Scandinavia using tracer gas dispersion, which obtained a range of $CH_4$ emission fluxes from 1.1 ± 0.1 to 18.1 ± 6.3 kg $h^{-1}$. Moore et al. (2023) employed an integrated Gaussian plume model with a Bayesian framework for mobile measurements of $CH_4$ emissions from 63 WWTPs in the United States, pointing to a significant underestimation in the $CH_4$ emission inventories.

We present a mobile measurement investigation of a WWTP in Hangzhou 2023. To analyze the mobile data, we construct a multi-source Gaussian plume model combined with the genetic algorithm inversion framework, which assists us to locate and quantify $CH_4$ emission sources, based on the concentration distribution measured within the WWTP. Additionally, we compare $CH_4$ emission fluxes from the measurements with the bottom-up estimates of emission inventories. A sensitivity analysis is performed to elucidate the discrepancies arising from variations in emission source locations. Our results provide insight into formulating and evaluating emission reduction measures for WWTPs.

## 2 Instruments and methods

### 2.1 Site selection

The monitoring site was chosen at a WWTP in Hangzhou, a megacity in East China.

https://doi.org/10.5194/egusphere-2024-2522
Preprint. Discussion started: 30 September 2024


This WWTP is a large-scale plant located in Hangzhou, processing up to 1.5 million tons of domestic wastewater daily. The plant roads were flat and wide, suitable for vehicle-mounted CRDS (Cavity Ring-Down Spectroscopy) to conduct monitoring along the internal roads of the plant to monitor various functional areas within the plant. WWTPs processes typically encompass mechanical treatment, biological treatment, sedimentation, advanced treatment, disinfection, and sludge treatment. As illustrated in Fig. 1, we divide the WWTP into 14 functional areas according to treatment processes. For instance, areas associated with primary treatment were labeled as coarse screens and primary sedimentation tanks, while those linked to secondary treatment were indicated as aeration tanks and secondary sedimentation tanks. Mobile measurements were conducted by driving around the outer periphery and internal functional areas of the wastewater treatment plant, with each monitoring experiment involving circling the functional areas 1-2 times. 10 days of experiments were carried out from June to December 2023. This yielded 8 valid sets of monitoring data, including 3 days of summer data and 5 days of winter data.


**Figure 1.** Distribution of functional areas of the WWTP. Map data are from ESRI.

https://doi.org/10.5194/egusphere-2024-2522
Preprint. Discussion started: 30 September 2024


## 2.2 Instrumentation

The monitoring instruments consisted of a vehicle-mounted CRDS monitoring system and a portable meteorological station. The vehicle-mounted CRDS system was anchored by the CRDS analyzer (Picarro G2201-i), accompanied by GPS and meteorological instruments. The CRDS analyzer measures $^{12}CO_2$, $^{13}CO_2$, $^{12}CH_4$, $^{13}CH_4$ and $H_2O$, the volume fraction of $CH_4$ is measured with an accuracy of 5 ppb ± 0.05 % (Picarro 2010). CRDS measurements have the advantages of strong interference resistance, high sensitivity and accuracy, making them widely employed in research focused on monitoring GHG emissions (Rella et al., 2015; Lopez et al., 2017). In this study, the CRDS analyzer was securely placed inside the monitoring vehicle, with the sampling probe mounted on the roof to mitigate the effects of vehicular emissions. The system was powered by a battery, drawing in ambient air through a pump, and displaying real-time monitoring data on a screen. The mobile meteorological instrument was placed on the roof of the vehicle to gather meteorological data. In addition, the GPS unit was integrated to record the location of sampling points during the measurement period.

Two portable meteorological stations (SWS-500) were positioned adjacent to the main entrance and atop the filter tank at the WWTP. Capable of measuring key meteorological parameters such as wind speed, direction, temperature, humidity, and atmospheric pressure, this station provided essential climatic data for the monitoring experiments. Mobile measurements were performed by the monitoring vehicle along the entire roads of the WWTP, as well as the internal roads, to pinpoint the locations of emission sources, scrutinize variations in emission concentrations. The concentration data was subsequently integrated with an inversion model to estimate the $CH_4$ emission fluxes.

https://doi.org/10.5194/egusphere-2024-2522
Preprint. Discussion started: 30 September 2024


## 2.3 Inventory accounting method

We used the methods suggested by the IPCC Guidelines for National Greenhouse Gas Inventories (2006) to calculate the amounts of $CH_4$ emissions from wastewater. The formula for calculating the amounts of $CH_4$ emissions from wastewater is described as:

$$E_{CH_4} = (TOW - S \cdot a) \cdot EF_{CH_4} - R_{CH_4} \quad (1)$$

Where $E_{CH_4}$ denotes the direct $CH_4$ emissions from the wastewater treatment plant, $tCH_4\ a^{-1}$. $TOW$ is defined as the total organic pollutant load in the influent wastewater, $tCOD\ a^{-1}$. $S$ refers to the annual production total of dry sludge, $t\ a^{-1}$. The parameter $a$ signifies the organic matter content in the dry sludge, $tCOD\ t^{-1}$. $EF_{CH_4}$ is the $CH_4$ emission factor, $tCH_4\ tCOD^{-1}$. $R_{CH_4}$ quantifies the annual recovery of $CH_4$ from anaerobic treatment processes, $t\ a^{-1}$.

Operational data of the WWTP examined in this study is derived from the Urban Drainage Statistical Yearbook, an annual publication of urban water supply and drainage systems in China. This data set includes details such as the water treatment volume, sludge production, and the concentrations of six pollutants ($COD_{Cr}$, BOD, SS, $NH_3$-N, TN, and TP) in both influent and effluent. The Total Organic Waste (TOW) is deduced from the yearbook's foundational data, while the annual sludge production (S) is extracted directly from it. The organic matter content in dry sludge is estimated at an empirical 40 %, assuming a sludge moisture content of 75 %, leading to a value of 0.1 (Guo et al., 2019). $EF_{CH_4}$ is selected based on the recommended value for Zhejiang province, 0.0046 (Cai et al., 2015). Given the infrequency of anaerobic treatment in wastewater, $R_{CH_4}$ is set to 0.

## 2.4 Inversion method

We developed an inversion framework for $CH_4$ emission fluxes designed for plant-

https://doi.org/10.5194/egusphere-2024-2522
Preprint. Discussion started: 30 September 2024


level applications. The framework used $CH_4$ concentration measurements, specific locations of emission sources, and initial emission estimates, alongside wind speed and direction data, as inputs to the multi-point and line source Gaussian diffusion models. The preliminary localization of the emission sources was chiefly contingent upon the concentration distribution along the roads within the internal functional areas. Meanwhile, the initial emission estimates for each source were determined by integrating the concentration data from these areas with an improved empirical equation (Weller et al., 2018). These inputs were fed into a multi-source Gaussian plume model that simulates the concentration patterns of $CH_4$ given multiple point and line sources. We then used a genetic algorithm to iteratively optimize source emission fluxes and their locations. The inversion framework simulation dictated the placement of 12 main point sources throughout the WWTP, specifically within Aeration Tank ①②③④⑤, Primary Clarifier ③④⑤, Screen ①, Secondary Clarifier ①②, and the Sludge Treatment ② (Fig. 1). The inclusion of a Gaussian line source model was determined based on the actual emission conditions. Within this study, a uniform line source was established, with the assumed location along the road between the Screen ① and the Primary Clarifier ①. This assumption was grounded in the $CH_4$ concentration distribution observed within this road segment and was substantiated through model validation, confirming the existence of a line source emission pattern. The remaining emission flux inversion processes followed the same procedure as the point source simulation. Adjustments to the source locations within the model narrow the gap between simulated and measured concentrations, thus enhancing the accuracy of inversion. This section delineates each model incorporated into the inversion framework.

https://doi.org/10.5194/egusphere-2024-2522
Preprint. Discussion started: 30 September 2024


### 2.4.1 Multiple-point-source Gaussian plume model

We developed a multiple-point-source Gaussian plume model to relate $CH_4$ concentration enhancement to $CH_4$ emissions. This method approximates atmospheric dispersion of $CH_4$ from an individual source as a Gaussian plume under uniform and stable wind conditions (Nassar et al., 2017), which is usually good for describing average atmospheric transport tens to hundreds of meters downwind the source, making the Gaussian plume model a useful tool to study emissions from industrial and traffic sources.

The mass concentration enhancement ($C$, mg m$^{-3}$) is computed as superposition of Gaussian plumes from multiple point sources.

$$C(x,y,z) = \sum_{i=1}^{n} \frac{Q_i}{2\pi\bar{u}\sigma_{i,y}\sigma_{i,z}} exp\left(-\frac{(y-y_i)^2}{2\sigma_{i,y}{}^2}\right)\left\{exp\left[\frac{-(z-z_i)^2}{2\sigma_{i,z}{}^2}\right] + exp\left[\frac{-(z+z_i)^2}{2\sigma_{i,z}{}^2}\right]\right\} \quad (2)$$

The variables $x$, $y$, and $z$ denote the downwind, crosswind distances, and the height above the ground from the source, m. $Q_i$ signifies the emission rate from the $i_{th}$ point source, mg/s, for $i$ = 1, 2, 3……N, where $N$ represents the total count of point sources. The average wind speed is indicated by $\bar{u}$, m s$^{-1}$. The $x_i$, $y_i$ and $z_i$ are represented as the spatial position of the $i_{th}$ point source, m. $\sigma_{i,y}$ and $\sigma_{i,Z}$ are the horizontal and vertical dispersion parameters of the $i_{th}$ point source, respectively, which are given by the formula below:

$$\sigma_{i,y} = \gamma_1 \cdot (x - x_i)^{\alpha_1}, \ when\ x > x_i \quad (3)$$

$$\sigma_{i,z} = \gamma_2 \cdot (x - x_i)^{\alpha_2}, \ when\ x > x_i \quad (4)$$

The power functions, known as the Pasquill's curves, associates with the downwind distance x and the prevailing atmospheric stability (Briggs et al., 1973). Atmospheric stability is determined based on the Pasquill stability classes recommended in the Technical Principles and Methods for Formulating Local Air Pollution Emission Standards (GB3840-83).

https://doi.org/10.5194/egusphere-2024-2522
Preprint. Discussion started: 30 September 2024


### 2.4.2 General Finite Line Source Model

Our analysis of measurement at WWTPs indicates that multiple-point-source Gaussian plume model is insufficient to capture the observed $CH_4$ concentrations. The entire road between the Screen ① and the Primary Clarifier ① shows high distribution of $CH_4$ concentrations. To match the observations, we further consider a line source based on observed concentration distribution. The line source model is used to confirm that the road concentration distribution is consistent with line source emissions (Fig. S1). The contribution of a line source to $CH_4$ concentration is given by the General Finite Line Source Model (GFLSM) (Luhar et al., 1989; Venkatram et al., 2006), which represents the line source as an ensemble of point sources:

$$C = \frac{Q}{2\pi\bar{u}\sigma_y\sigma_z}\left\{exp\left[\frac{-(z-H)^2}{2{\sigma_z}^2}\right] + exp\left[\frac{-(z+H)^2}{2{\sigma_z}^2}\right]\right\} \cdot\left[erf\left(\frac{\sin\theta\left(\frac{L}{2}-y\right)-x\cos\theta}{\sqrt{2}\sigma_y}\right) + erf\left(\frac{\sin\theta\left(\frac{L}{2}+y\right)+x\cos\theta}{\sqrt{2}\sigma_y}\right)\right] \quad (5)$$

$x$, $y$, and $z$ correspond to the downwind, crosswind distances, and the altitude above ground level from the source, m. $Q_i$ is the emission fluxes of the unit source, mg $s^{-1}$. $\bar{u}$ is the average wind speed, m $s^{-1}$. $H_i$ is the effective emission height of the line source, with the length of the line source represented by $L$, m. The angle between the line source and the wind direction is given by $\theta$. The horizontal and vertical dispersion parameters are characterized by $\sigma_y$ and $\sigma_z$, respectively.

### 2.4.2 Genetic algorithm

Genetic algorithms, which mimic the evolutionary process of biological systems, serve as optimization search algorithms. The algorithms encode practical problems into binary genetic coding. Through the simulation of natural selection, crossover, and mutation processes, these algorithms are in a constant state of evolution and iteration,

https://doi.org/10.5194/egusphere-2024-2522
Preprint. Discussion started: 30 September 2024


all in the pursuit of the optimal solution (Katoch et al., 2021). We deployed genetic algorithms to enhance the source emission flux outcomes modeled by the Gaussian plume model.

The process of inverting multi-source $CH_4$ emission fluxes utilizing genetic algorithms involves a series of steps. Initially, the emission flux of each source is treated as a gene, with binary-encoded gene sequences randomly assigned to a set number of individuals within the predefined range of a priori emission fluxes. Subsequently, the formulation of a fitness function is based on the defined optimization goals and constraints. This function serves as a critical tool for assessing the relative merits of each individual within the population. In this study, the objective of the optimization is centered on minimizing the aggregate absolute discrepancy between the values predicted by the model and those obtained from measurements. Ultimately, the population is subjected to the processes of selection, crossover, and mutation. Individuals with elevated fitness values, as determined by the fitness function, are chosen for the generation of new individuals. Through an iterative process, the optimal solution is refined, representing the emission fluxes for each source. Genetic algorithms are distinguished by the parallel computation capabilities, the propensity for identifying global optima, and the commendable stability and reliability (Harada et al., 2020).

## 3 Results and discussion

### 3.1 Concentration mapping

The closed-path mobile measurements were conducted by vehicle-mounted CRDS monitoring system along the external roads encircling the WWTP, with further monitoring conducted along the internal roads. This strategy depicts the distribution of $CH_4$ concentrations within an WWTP, allowing for identification of specific $CH_4$ emission sources. Based on 8 days of $CH_4$ monitoring experimental data, the $CH_4$

https://doi.org/10.5194/egusphere-2024-2522
Preprint. Discussion started: 30 September 2024


concentration range on the overall roads was determined to be 1.98-17.13 ppm. The $CH_4$ concentration distribution indicated higher levels downwind, with the highest concentrations consistently recorded at the Screen ① throughout mobile experiments.

Due to the similarity of concentration measurement methods, we chose 29$^{th}$ June and 13$^{th}$ December as a typical example for measuring the spatial distribution of $CH_4$ and evaluating the seasonal variability of WWTP. Figure 2 illustrates measured $CH_4$ concentration enhancement distributions on 29$^{th}$ June (summer) and 13$^{th}$ December (winter) 2023 (other days are shown in Figures S2-S7). The $CH_4$ concentration enhancements depicted within the figures were calculated by subtracting the background concentrations from the measured values, with the background determined as the mean of the bottom 10 % of the concentration data. Specifically, the background concentrations register at 1.98 ppm on 29$^{th}$ June and at a slightly elevated 2.11 ppm on 13$^{th}$ December. Moreover, increased concentrations are detected in the regions surrounding the Screen ①, Primary Clarifier ④, and Aeration Tank ③ during these two days. The complete concentration maps , which include the internal roads, reveal that the experiment on 29$^{th}$ June exhibits heightened concentrations at the Screen ①, Secondary Clarifier ②, and Primary Clarifier ②④. The Screen ① exhibits the highest $CH_4$ concentration, with an enhancement of 14.83 ppm. On 13$^{th}$ December, the concentration enhancements are noted in proximity to the Secondary Clarifier ① and Primary Clarifier ②, with the Primary Clarifier ② showing the highest $CH_4$ concentration at 4.79 ppm.

$CH_4$ concentrations in summer surpass those observed in winter, consistent with a previous study on WWTPs (Masuda et al., 2015). The screen, primary clarifier and aeration tank are identified as sources with notably higher concentrations. Analysis of concentration distributions reveals that Screen ① shows a peak concentration reaching 14.83 ppm, which is 7.5 times the background concentration. The four primary

https://doi.org/10.5194/egusphere-2024-2522
Preprint. Discussion started: 30 September 2024


clarifiers record high concentrations between 4.79 and 10.88 ppm. The high value measured by aeration tanks is mainly detected in Aeration Tank ③ at 4.60ppm. The screen in this study includes coarse and fine screens and a grit chamber, constituting preliminary wastewater treatment to capture larger suspended solids and particulates. The anaerobic environment of the sewer network promotes the production of $CH_4$ from organic compounds in municipal wastewater. As this wastewater enters the WWTP, the influent contains dissolved $CH_4$ that originated in the sewer network. During primary treatment, wastewater is elevated through riser mains, facilitating the release of $CH_4$ into the atmosphere (Guisasola et al., 2008; Bao et al., 2016). Flow velocity, hydraulic design and detention times in these facilities may affect $CH_4$ production and release (Alshboul et al., 2016; Yin et al., 2024). The primary clarifier physically removes suspended solids from wastewater through sedimentation, while organic matter undergoes anaerobic microbial degradation to the substantial production of $CH_4$ (Masuda et al., 2017). In the aeration tank, operated under anaerobic and anoxic conditions, complex organic compounds are converted to $CH_4$ by facultative and anaerobic bacteria through biological processes (Yoshida et al.,2014). In contrast, Kupper et al. (2018) identified sludge storage tanks as the primary source of $CH_4$ emissions in Swiss WWTPs, accounting for 70 % or more of the total emissions. Stadler et al. (2022) monitored $CH_4$ concentrations inside and around wastewater treatment facilities ranging from 2.04-32.78 ppm, with elevated $CH_4$ levels predominantly measured near sludge treatment tank, the digesters and secondary clarifiers.

https://doi.org/10.5194/egusphere-2024-2522
Preprint. Discussion started: 30 September 2024


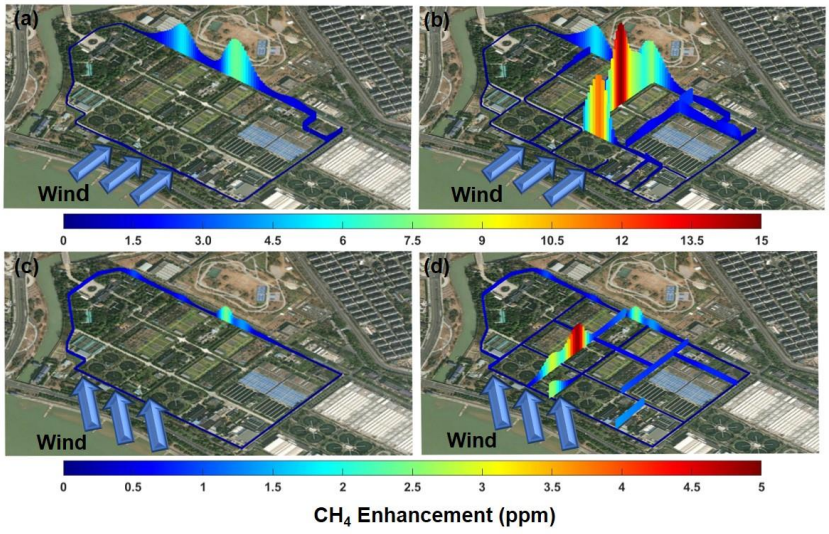


**Figure 2.** $CH_4$ concentration maps in the WWTP. The concentration maps for the external roads for 29th June (a) and 13th December (c). The corresponding complete concentration maps that include the internal roads for 29th June (b) and 13th December (d). Map data are from ESRI.

### 3.2 Emission quantification

The mobile measured $CH_4$ concentrations were employed in combination with the inversion framework to achieve the quantification of $CH_4$ emissions and localization of the emission sources within the WWTP. Figures 3 and 4 show the locations of identified point sources and the comparison between monitored and simulated concentrations for the point source locations at the WWTP on the dates of 29th June and 13th December. The experiment conducted on 29th June finds the Screen ① to be the most significant contributor to $CH_4$ point source emissions at 160.19 t $a^{-1}$, and the Secondary Clarifier ② as the least significant at 10.78 t $a^{-1}$. The correlation coefficient $R^2$ for the monitored and simulated concentrations is 0.63, with an RMSE of 0.70 mg $m^{-3}$. On 13th December,

https://doi.org/10.5194/egusphere-2024-2522
Preprint. Discussion started: 30 September 2024


the Aeration Tank ⑤ is the largest point source of $CH_4$ emissions at 34.48 t $a^{-1}$, and the Primary Clarifier ⑤ is the smallest at 4.82 t $a^{-1}$, with a correlation coefficient $R^2$ of 0.70 and an RMSE of 0.28 mg $m^{-3}$. The enhanced correlation between winter monitoring and simulation data, as well as the improved fit of the monitoring and simulation value curves, is attributed to the shorter monitoring cycle and more stable meteorological conditions.

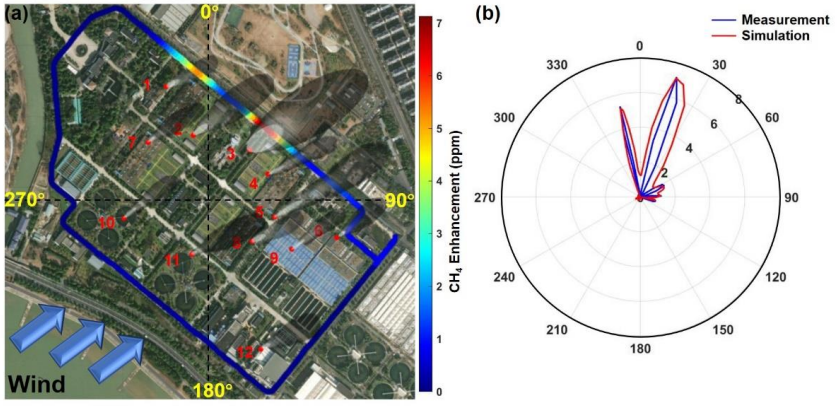


**Figure 3.** The emission distribution for the source locations (a) and the comparison between monitored and simulated $CH_4$ concentrations (b) at the WWTP on 29th June. Map data are from ESRI.

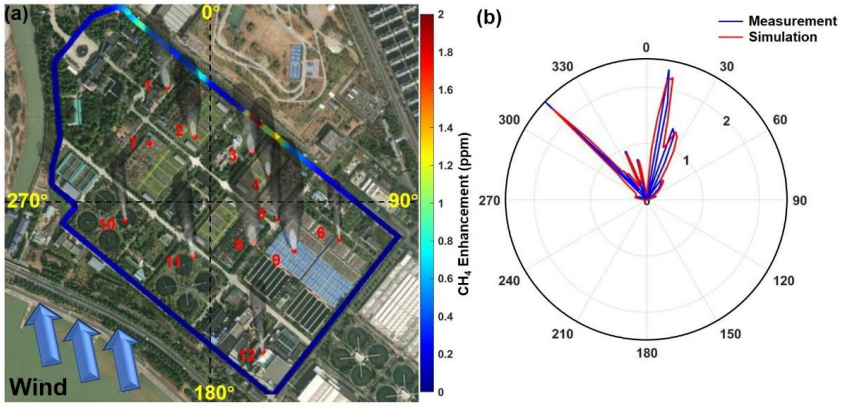


**Figure 4.** The emission distribution for the source locations (a) and the comparison

https://doi.org/10.5194/egusphere-2024-2522
Preprint. Discussion started: 30 September 2024


between monitored and simulated $CH_4$ concentrations (b) at the WWTP on 13th December. Map data are from ESRI.

Table 1 displays the $CH_4$ emission fluxes, meteorological data, and the coefficients of the power function expressions for diffusion parameters from the 8-day monitoring experiment. The emission flux values of $CH_4$ emission sources (12 point sources and 1 line source) for all experimental days are detailed in Tables S1 and S2. It is observed that the summer average $CH_4$ emission flux ($603.33 \pm 152.66$ t $a^{-1}$) surpasses the winter average $CH_4$ emission flux ($418.95 \pm 187.59$ t $a^{-1}$). This seasonal disparity in emissions is primarily attributed to the aeration tank, followed by the screen and primary clarifier. The activated sludge in the aeration tank contains a higher population of methanogens, whose $CH_4$ production capability intensifies with rising temperatures (Vítěz et al., 2020). Notably, the seasonal variance in the aeration tank is predominantly driven by the performance of the Aeration Tank ④. However, the substantial variation in the emissions from the three summer experiments of the Aeration Tank ④ suggests a degree of emission instability. Conversely, the uniformity in the low emissions from the five winter experiments might be associated with the meteorological conditions and the actual operational status of the plant on those days.

Analysis of emission source data from Tables S1 and S2 reveals that the screen and primary clarifier are the predominant emission sources at the WWTP. Specifically, these sources emit 329 t $a^{-1}$ in the summer and 280 t $a^{-1}$ in the winter, accounting for 55 % and 67 % of the total emissions. The study hypothesizes that emissions are boosted by pipeline leaks near the emission sources in the screen and primary clarifier, leading to more $CH_4$ release. Previous research has similarly examined major emission sources at WWTPs. Yin et al. (2024) conducted offline monitoring of WWTPs in Beijing and Guiyang, identifying the primary treatment zone as the primary source of $CH_4$, accounting for 60.1 % and 35.8 % of the respective total emissions. Masuda et al. (2017)

https://doi.org/10.5194/egusphere-2024-2522
Preprint. Discussion started: 30 September 2024


analyzed $CH_4$ emissions from different processes at three WWTPs in Japan, concluding that primary clarifiers are one of the major sources of $CH_4$ emissions. He et al. (2023) compiled $CH_4$ emission proportions for different processes in WWTPs based on reported data, finding percentages of 7 %-12 % for grit chamber, 8.2 %-68.1 % for primary clarifier, and 18.3 %-86.4 % for aeration tank.

**Table 1.** $CH_4$ emission fluxes, meteorological data and diffusion parameter power function expression coefficients from the 8-day monitoring experiment.

| Date | Q (t $a^{-1}$) | $W_s$ (m $s^{-1}$) | $W_d$ (°) | $\gamma_1$ | $\alpha_1$ | $\gamma_2$ | $\alpha_2$ |
|---|---|---|---|---|---|---|---|
| 0601 | 542.50 ± 179.03 | 2.3 | 248.5 | 0.28 | 0.91 | 0.13 | 0.94 |
| 0629 | 657.18 ± 308.88 | 1.9 | 238.3 | 0.28 | 0.91 | 0.13 | 0.94 |
| 0711 | 610.31 ± 286.85 | 0.9 | 225.8 | 0.28 | 0.91 | 0.13 | 0.94 |
| 1213 | 431.51 ± 185.55 | 1.6 | 175.7 | 0.28 | 0.91 | 0.13 | 0.94 |
| 1214 | 379.77 ± 239.26 | 1.2 | 209.9 | 0.28 | 0.91 | 0.13 | 0.94 |
| 1220 | 438.55 ± 219.28 | 3.8 | 342.3 | 0.18 | 0.92 | 0.11 | 0.92 |
| 1221 | 422.53 ± 152.11 | 2.7 | 342.6 | 0.43 | 1.10 | 0.08 | 1.12 |
| 1222 | 422.40 ± 190.08 | 3.0 | 342.5 | 0.43 | 1.10 | 0.08 | 1.12 |

### 3.3 Comparison with IPCC method

The direct $CH_4$ emissions from WWTP were calculated using the IPCC method, with data sourced from the Urban Drainage Statistical Yearbook of 2017. By applying the formula to the basic information of the WWTP outlined in the yearbook, the emission flux of 213.95 ± 128.37 t $a^{-1}$ was determined, with the uncertainty derived from the data summarized in the research (Lin et al., 2021). Figure 5 shows the contrast between the emission inversion results from the monitoring experiment and the emission inventory. The uncertainty of the inversion results was determined by the uncertainties in wind speed, wind direction, and instrument measurements. The summer average inversion

https://doi.org/10.5194/egusphere-2024-2522
Preprint. Discussion started: 30 September 2024


emission flux (603.33 ± 152.66 t $a^{-1}$) was calculated to be 2.8 times that of the inventory, and the winter average (418.95 ± 187.59 t $a^{-1}$) was twice as much. It is posited that the discrepancy may stem from significant uncertainties in the emission factors associated with the WWTPs or the lack of updated activity level data, as the statistical yearbook provided data only up to 2017, the emission inventory might have underestimated the actual emissions.

Furthermore, other studies have also investigated the comparison between $CH_4$ emissions obtained from different measurement methods at WWTPs and IPCC inventory estimates. The majority of these studies indicate that the measured values exceed the inventory values. Wang et al. (2021) conducted a measurement-based assessment of $CH_4$ emissions (46.58 t $a^{-1}$) in Wuhu City, revealing a 46.71 % higher than those calculated using the IPCC method. Moore et al. (2023) employed mobile monitoring to evaluate $CH_4$ emissions at 63 WWTPs across the United States. The study showed that the estimates based on the IPCC guidelines underestimated the emissions from most of the measured plants. Specifically, $CH_4$ emissions from centrally treated domestic wastewater in the U.S. amount to $4.64\times10^5$ t $a^{-1}$, which is 1.9 times greater than the EPA inventory. Song et al. (2023) investigated $CH_4$ emissions from sewer systems and water resource recovery facilities. Utilizing a collected dataset, they employed the Monte Carlo analysis method to determine the $CH_4$ emissions from municipal wastewater treatment in the U.S. at $(4.36 \pm 2.8) \times 10^5$ t $a^{-1}$. This value was approximately twice the estimates provided by the IPCC. The lower estimated results provided by the IPCC method can be attributed to the neglect of certain potential emission sources from the emission inventories, including emissions from equipment in sludge treatment facilities and leaks from pressure relief valves.

https://doi.org/10.5194/egusphere-2024-2522
Preprint. Discussion started: 30 September 2024


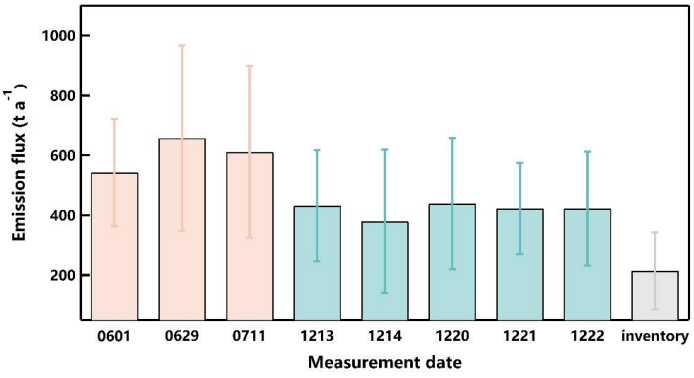


451

452 **Figure 5.** Comparison of $CH_4$ emission fluxes from the monitoring experiment and
453 emission inventory in the WWTP.

454 **3.4 Sensitivity analysis**

455 In this section, we evaluated the stability of the inversion framework through
456 sensitivity analysis and explored the impact of different point source locations on the
457 inversion of emission concentrations. The precise identification of emission sources can
458 enhance the accuracy of emission flux inversion, making a sensitivity analysis of the
459 source location essential. We applied the method of controlling variables to perform a
460 sensitivity analysis on the location of a single point source. The central position of the
461 plant was taken as the reference origin, the positions of 12 emission sources were
462 determined to analyze the variation in error between measured and simulated
463 concentrations within a 200 m × 200 m range around each emission source. We
464 sequentially modified the source position parameters in the model input to analyze the
465 congruence between the simulated concentrations and the observed measurements,
466 quantifying the fit with RMSE. The change in concentration error serves as an indicator
467 of the accuracy of the emission source localization.

468 Figures 6 and 7 describe the error variation between monitored and simulated
469 concentrations when the point source location is subject to change within a 200 m ×
470 200 m range from the monitoring experiment on 29$^{th}$ June and 13$^{th}$ December. The error

https://doi.org/10.5194/egusphere-2024-2522
Preprint. Discussion started: 30 September 2024


variation of the remaining days can be seen in Figures S8-S13. The point source locations simulated based on the inversion framework are mostly in areas with minor relative concentration errors, which can be considered to have a high reliability in simulating point source locations. The emission source location errors for the two experiments are within the ranges of 0.7-1.3 mg $m^{-3}$ and 0.2-0.3 mg $m^{-3}$. The winter emission source locations exhibit greater stability and accuracy in the inversion results than the summer ones.

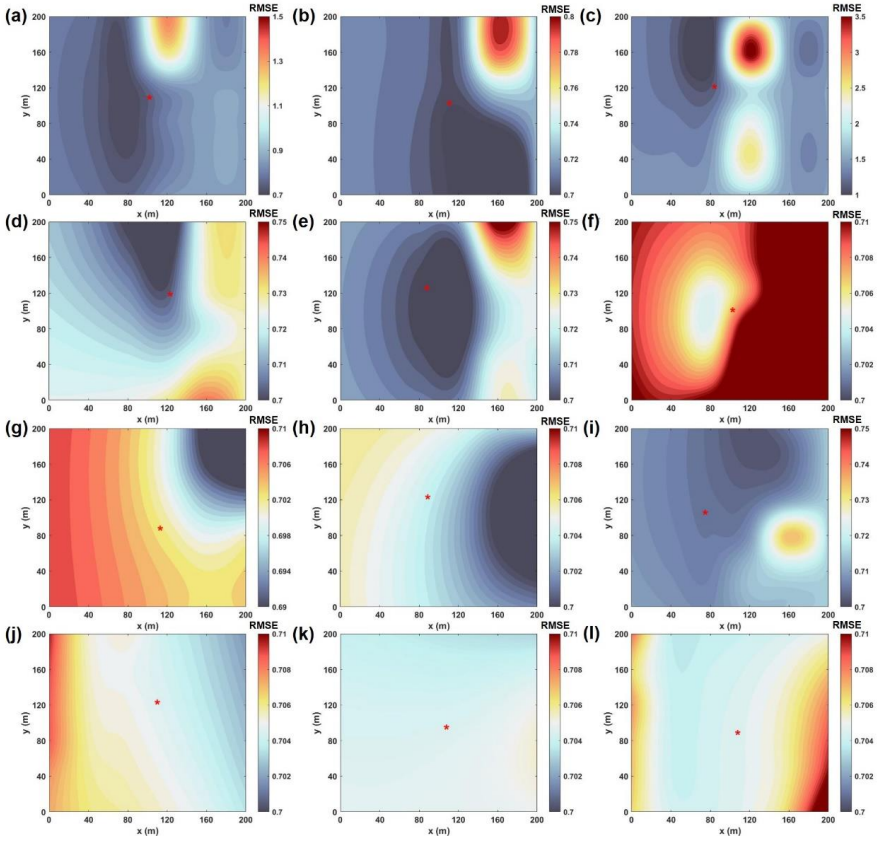


**Figure 6.** RMSE of monitoring simulated concentration changes with the location of WWTP source on 29th June. The x and y axes denote the horizontal and vertical distances of the simulated point source from the central point of the WWTP. The variation in color signifies the alteration in the root mean square error between the

https://doi.org/10.5194/egusphere-2024-2522
Preprint. Discussion started: 30 September 2024


actual monitored and simulated concentrations, with the red star symbolizing the simulated point source location.

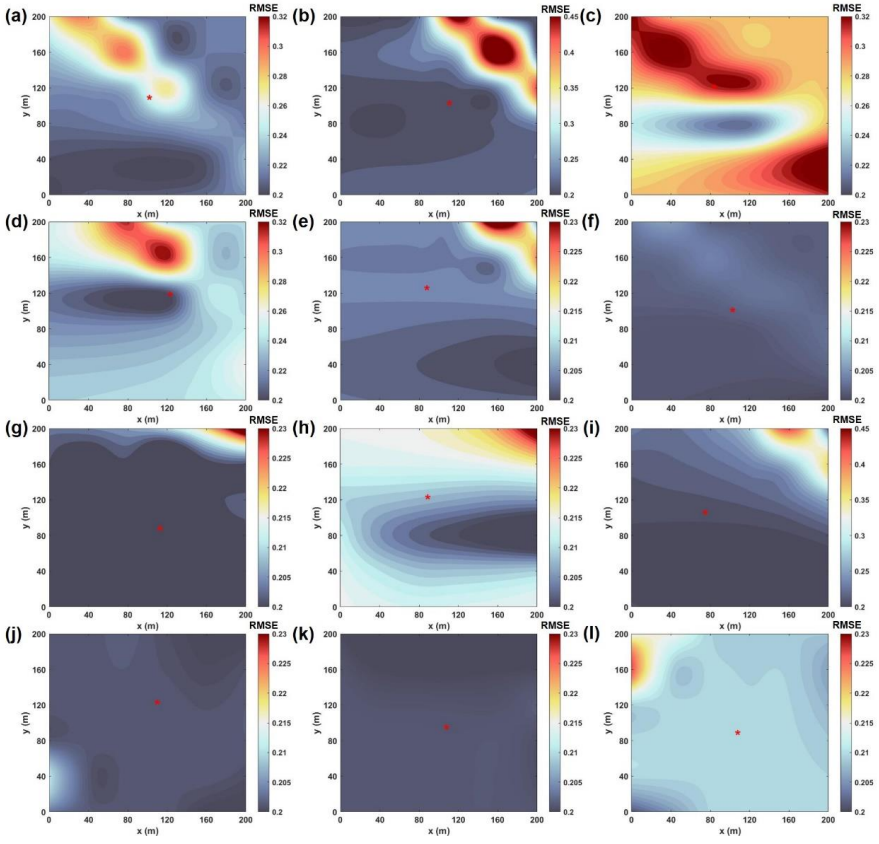


**Figure 7.** RMSE of monitoring simulated concentration changes with the location of WWTP source on 13th December.

## 4 Conclusions and outlook

The study carried out CRDS mobile measurements at a WWTP across the summer and winter seasons from Hangzhou 2023. By employing a multi-source Gaussian plume model combined with the genetic algorithm inversion framework, the inversion of $CH_4$ emission fluxes and their source locations was achieved. A sensitivity analysis of the

https://doi.org/10.5194/egusphere-2024-2522
Preprint. Discussion started: 30 September 2024


parameters within the inversion framework was conducted to verify the reliability of the model, offering a strategic approach for the quantification of GHG emissions at the plant scale. The results showed that 12 distinct $CH_4$ emission sources were pinpointed within the facility through the inversion framework. The average $CH_4$ emission flux during the summer was calculated to be 603.33 ± 152.66 t $a^{-1}$, and 418.95 ± 187.59 t $a^{-1}$ for the winter. The screen and primary clarifier were the main sources, accounting for 55 % of summer and 67 % of winter emissions. When contrasted with bottom-up emission inventory estimates, the summer $CH_4$ inversion emissions were found to be 2.8 times higher, and the winter inversion emissions were twice as much as the inventory values.

The inversion framework is capable of validating emission coefficients in the inventory, identifying emission sources within the plant, and monitoring abnormal emissions. It can be applied to various monitoring systems, such as UAV systems and networks of fixed monitoring stations. We believe that collaborative monitoring by different methods can significantly improve the accuracy of emission fluxes and emission sources inversions. It is suggested that future endeavors focus on refining the inversion framework for broader applicability to various pollutant gases, enhancing the inversion efficiency, and extending the validation of the framework through monitoring experiments in a diverse range of industrial facilities.

***Data availability.*** The raw data in this paper can be obtained from the corresponding author upon request.

***Author contributions.*** ZW and YZ administrated the project and determined the main goal of this study. ZX, JY and XP designed the methods and planned the campaign. JY, ZX, YY, SZ and BQ performed the measurements. JY wrote the paper with contributions from all co-authors.

***Competing interests.*** At least one of the (co-)authors is a member of the editorial board

https://doi.org/10.5194/egusphere-2024-2522
Preprint. Discussion started: 30 September 2024


of Atmospheric Chemistry and Physics.

***Financial support.*** The study has been supported by the National Key Research and Development Program of China (grant nos. 2022YFC3703500 and 2022YFE0209100), the National Natural Science Foundation of China (grant no. 42307129), the Key Research and Development Program of Zhejiang Province (grant nos. 2021C03165 and 2022C03084), the Zhejiang Provincial Natural Science Foundation (grant no. LZJMZ24D050005), and the Ecological Environment Research and Achievement Promotion Project of Zhejiang Province (grant nos. 2024XM0053 and 2024XM0052).

## References

Abeywickrama, H. G. K., Bajón-Fernández, Y., Srinamasivayam, B., Turner, D., and Rivas Casado, M.: Development of a UAV based framework for $CH_4$ monitoring in sludge treatment centres, Remote Sens., 15, 3704, https://doi.org/10.3390/rs15153704, 2023.

Albertson, J. D., Harvey, T., Foderaro, G., Zhu, P., Zhou, X., Ferrari, S., Amin, M. S., Modrak, M., Brantley, H., and Thoma, E. D.: A Mobile Sensing Approach for regional surveillance of fugitive methane emissions in oil and gas production, Environ. Sci. Technol., 50, 2487-2497, https://doi.org/10.1021/acs.est.5b05059, 2016.Allen, G., Hollingsworth, P., Kabbabe, K., Pitt, J. R., Mead, M. I., Illingworth, S., Roberts, G., Bourn, M., Shallcross, D. E., and Percival, C. J.: The development and trial of an unmanned aerial system for the measurement of methane flux from landfill and greenhouse gas emission hotspots, Waste Manage., 87, 883-892, https://doi.org/10.1016/j.wasman.2017.12.024, 2019.

Al-Shalan, A., Lowry, D., Fisher, R. E., Nisbet, E. G., Zazzeri, G., Al-Sarawi, M., France, J. L.: Methane emissions in Kuwait: Plume identification, isotopic characterisation and inventory verification, Atmos. Environ., 268, 118763, https://doi.org/10.1016/j.atmosenv.2021.118763, 2022.

https://doi.org/10.5194/egusphere-2024-2522
Preprint. Discussion started: 30 September 2024


Alshboul, Z., Encinas-Fernández, J., Hofmann, H., and Lorke, A.: Export of dissolved methane and carbon dioxide with effluents from municipal wastewater treatment plants, Environ. Sci. Technol., 50, 5555-5563, https://doi.org/10.1021/acs.est.5b04923, 2016.

Bai, R. L., Jin, L., Sun, S. R., Cheng, Y., and Wei, Y.: Quantification of greenhouse gas emission from wastewater treatment plants, Greenhouse. Gas. Sci. Technol., 12, 587-601, https://doi.org/10.1002/ghg.2171, 2022.

Balashov, N. V., Davis, K. J., Miles, N. L., Lauvaux, T., Richardson, S. J., Barkley, Z. R., and Bonin, T. A.: Background heterogeneity and other uncertainties in estimating urban methane flux: results from the Indianapolis Flux Experiment (INFLUX), Atmos. Chem. Phys., 20, 4545-4559, https://doi.org/10.5194/acp-20-4545-2020, 2020.

Bao, Z., Sun, S., and Sun, D.: Assessment of greenhouse gas emission from A/O and SBR wastewater treatment plants in Beijing, China. Int. Biodeterior. Biodegrad., 108, 108-114, https://doi.org/10.1016/j.ibiod.2015.11.028, 2016.

Bergamaschi, P., Karstens, U., Manning, A. J., Saunois, M., Tsuruta, A., Berchet, A., Vermeulen, A. T., Arnold, T., Janssens-Maenhout, G., Hammer, S., Levin, I., Schmidt, M., Ramonet, M., Lopez, M., Lavric, J., Aalto, T., Chen, H., Feist, D. G., Gerbig, C., Haszpra, L., Hermansen, O., Manca, G., Moncrieff, J., Meinhardt, F., Necki, J., Galkowski, M., O'Doherty, S., Paramonova, N., Scheeren, H. A., Steinbacher, M., and Dlugokencky, E.: Inverse modelling of European $CH_4$ emissions during 2006–2012 using different inverse models and reassessed atmospheric observations, Atmos. Chem. Phys., 18, 901-920, https://doi.org/10.5194/acp-18-901-2018, 2018.

Cai, B., Gao, Q., Li, Z., Wu, J., Cao, D., and Liu, L.: Study on the methane emission factors of wastewater treatment plants in China, China Population Resources and Environment, 25, 118-124, https://doi.org/10.3969/j.issn.1002-2104.2015.04.015, 2015.

Caulton, D. R., Li, Q., Bou-Zeid, E., Fitts, J. P., Golston, L. M., Pan, D., Lu, J., Lane,

https://doi.org/10.5194/egusphere-2024-2522
Preprint. Discussion started: 30 September 2024


H. M., Buchholz, B., Guo, X., McSpiritt, J., Wendt, L., and Zondlo, M. A.: Quantifying uncertainties from mobile-laboratory-derived emissions of well pads using inverse Gaussian methods, Atmos. Chem. Phys., 18, 15145-15168, https://doi.org/10.5194/acp-18-15145-2018, 2018.

Chen, J., Dietrich, F., Maazallahi, H., Forstmaier, A., Winkler, D., Hofmann, M. E. G., Denier van der Gon, H., and Röckmann, T.: Methane emissions from the Munich Oktoberfest, Atmos. Chem. Phys., 20, 3683-3696, https://doi.org/10.5194/acp-20-3683-2020, 2020.

Cui, Y. Y., Brioude, J., Angevine, W. M., Peischl, J., McKeen, S. A., Kim, S.-W., Neuman, J. A., Henze, D. K., Bousserez, N., Fischer, M. L., Jeong, S., Michelsen, H. A., Bambha, R. P., Liu, Z., Santoni, G. W., Daube, B. C., Kort, E. A., Frost, G. J., Ryerson, T., Wofsy, S. C., and Trainer, M.: Top-down estimate of methane emissions in California using a mesoscale inverse modeling technique: The San Joaquin Valley, J. Geophys. Res., 122, 3686–3699, https://doi.org/10.1002/2016JD026398, 2017.

Cusworth, D. H., Duren, R. M., Ayasse, A. K., Jiorle, R., Howell, K., Aubrey, A., Green, R. O., Eastwood, M. L., Chapman, J. W., Thorpe, A. K., Heckler, J., Asner, G. P., Smith, M. L., Thoma, E., Krause, M. J., Heins, D., and Thorneloe, S.: Quantifying methane emissions from United States landfills, Science, 383, 1499-1504, https://www.science.org/doi/10.1126/science.adi7735, 2024.

Defratyka, S. M., Paris, J. D., Yver-Kwok, C., Fernandez, J. M., Korben, P., and Bousquet, P.: Mapping Urban Methane Sources in Paris, France, Environ. Sci. Technol., 55, 8583-8591, https://doi.org/10.1021/acs.est.1c00859, 2021.

Delre, A., Mønster, J., and Scheutz, C.: Greenhouse gas emission quantification from wastewater treatment plants, using a tracer gas dispersion method, Sci. Total. Environ., 605-606, 258-268, http://dx.doi.org/10.1016/j.scitotenv.2017.06.177, 2017.

Dietrich, F., Chen, J., Voggenreiter, B., Aigner, P., Nachtigall, N., and Reger, B.: MUCCnet: Munich Urban Carbon Column network, Atmos. Meas. Tech., 14, 1111-1126, https://doi.org/10.5194/amt-14-1111-2021, 2021.

https://doi.org/10.5194/egusphere-2024-2522
Preprint. Discussion started: 30 September 2024


607 Guisasola, A., de Haas, D., Keller, J., and Yuan, Z.: Methane formation in sewer systems.
608 Water Res., 42, 1421-1430, https://doi.org/10.1016/j.watres.2007.10.014, 2008.
609 Guo, S., Huang, H., Dong, X., and Zeng, S.: Calculation of greenhouse gas emissions
610 of municipal wastewater treatment and its temporal and spatial trend in China, Water
611 & Wastewater Engineering, 45, 56-62, https://doi.org/10.13789/j.cnki.wwe1964.
612 2019.04.009, 2019.
613 Hase, F., Frey, M., Blumenstock, T., Groß, J., Kiel, M., Kohlhepp, R., Mengistu Tsidu,
614 G., Schäfer, K., Sha, M. K., and Orphal, J.: Application of portable FTIR
615 spectrometers for detecting greenhouse gas emissions of the major city Berlin, Atmos.
616 Meas. Tech., 8, 3059-3068, https://doi.org/10.5194/amt-8-3059-2015, 2015.
617 Han, G., Pei, Z., Shi, T., Mao, H., Li, S., Mao, F., Ma, X., Zhang, X., and Gong, W.:
618 Unveiling unprecedented methane hotspots in China's leading coal production hub:
619 A satellite mapping revelation. Geophys. Res. Lett., 51, e2024GL109065,
620 https://doi.org/10.1029/2024GL109065, 2024.
621 Heerah, S., Frausto-Vicencio, I., Jeong, S., Marklein, A. R., Ding, Y., Meyer, A. G.,
622 Parker, H. A., Fischer, M. L., Franklin, J. E., Hopkins, F. M., and Dubey, M.: Dairy
623 methane emissions in California's San Joaquin Valley inferred with ground-based
624 remote sensing observations in the summer and winter, J. Geophys. Res-Atmos., 126,
625 e2021JD034785. https://doi.org/10.1029/2021JD03478, 2021.
626 Harada, T., and Alba, E.: Parallel Genetic Algorithms: A Useful Survey, ACM Comput.
627 Surv., 53, 1-39, https://doi.org/10.1145/3400031, 2020.
628 He, Y., Li, Y., Li, X., Liu, Y., Wang, Y., Guo, H., Hou, J., Zhu, T., and Liu, Y.: Net-zero
629 greenhouse gas emission from wastewater treatment: Mechanisms, opportunities and
630 perspectives, Renew. Sust. Energ. Rev., 184, 113547, https://doi.org/10.1016/j.rser.
631 2023.113547, 2023.
632 IPCC: Climate Change 2023: Synthesis Report. Contribution of Working Groups I, II
633 and III to the Sixth Assessment Report of the Intergovernmental Panel on Climate
634 Change, 35-115, https://doi.org/10.59327/IPCC/AR6-9789291691647, 2023.

https://doi.org/10.5194/egusphere-2024-2522
Preprint. Discussion started: 30 September 2024


635 Jackson, R. B., Down, A., Phillips, N. G., Ackley, R. C., Cook, C. W., Plata, D. L., and
636 Zhao, K.: Natural gas pipeline leaks across Washington, DC, Environ. Sci. Technol.,
637 48, 2051-2058, https://doi.org/10.1021/es404474x, 2014.
638 Jacob, D. J., Varon, D. J., Cusworth, D. H., Dennison, P. E., Frankenberg, C., Gautam,
639 R., Guanter, L., Kelley, J., McKeever, J., Ott, L. E., Poulter, B., Qu, Z., Thorpe, A.
640 K., Worden, J. R., and Duren, R. M.: Quantifying methane emissions from the global
641 scale down to point sources using satellite observations of atmospheric methane,
642 Atmos. Chem. Phys., 22, 9617–9646, https://doi.org/10.5194/acp-22-9617-2022,
643 2022.
644 Karion, A., Lauvaux, T., Lopez Coto, I., Sweeney, C., Mueller, K., Gourdji, S.,
645 Angevine, W., Barkley, Z., Deng, A., Andrews, A., Stein, A., and Whetstone, J.:
646 Intercomparison of atmospheric trace gas dispersion models: Barnett Shale case
647 study, Atmos. Chem. Phys., 19, 2561-2576, https://doi.org/10.5194/acp-19-2561-
648 2019, 2019.
649 Katoch, S., Chauhan, S.S. and Kumar, V.: A review on genetic algorithm: past, present,
650 and future. Multimed. Tools Appl., 80, 8091-8126, https://doi.org/10.1007/s11042-
651 020-10139-6, 2021.
652 Kumar, P., Broquet, G., Yver-Kwok, C., Laurent, O., Gichuki, S., Caldow, C., Cropley,
653 F., Lauvaux, T., Ramonet, M., Berthe, G., Martin, F., Duclaux, O., Juery, C., Bouchet,
654 C., and Ciais, P.: Mobile atmospheric measurements and local-scale inverse
655 estimation of the location and rates of brief $CH_4$ and $CO_2$ releases from point sources,
656 Atmos. Meas. Tech., 14, 5987-6003, https://doi.org/10.5194/amt-14-5987-2021,
657 2021.
658 Li, H., You, L., Du, H., Yu, B., Lu, L., Zheng, B., Zhang, Q., He, K., and Ren, N.:
659 Methane and nitrous oxide emissions from municipal wastewater treatment plants in
660 China: A plant-level and technology-specific study, Environ. Sci. Technol., 20,
661 100345, https://doi.org/10.1016/j.ese.2023.100345, 2024.
662 Liang, R., Zhang, Y., Chen, W., Zhang, P., Liu, J., Chen, C., Mao, H., Shen, G., Qu, Z.,

https://doi.org/10.5194/egusphere-2024-2522
Preprint. Discussion started: 30 September 2024


Chen, Z., Zhou, M., Wang, P., Parker, R. J., Boesch, H., Lorente, A., Maasakkers, J.D., and Aben, I.: East Asian methane emissions inferred from high-resolution inversions of GOSAT and TROPOMI observations: a comparative and evaluative analysis, Atmos. Chem. Phys., 23, 8039-8057, https://doi.org/10.5194/acp-23-8039-2023, 2023.

Lin, X., Zhang, W., Crippa, M., Peng, S., Han, P., Zeng, N., Yu, L., and Wang, G.: A comparative study of anthropogenic $CH_4$ emissions over China based on the ensembles of bottom-up inventories, Earth Syst. Sci. Data, 13, 1073-1088, https://doi.org/10.5194/essd-13-1073-2021, 2021.

Lopez, M., Sherwood, O. A., Dlugokencky, E. J., Kessler, R., Giroux, L., and Worthy, D. E. J.: Isotopic Signatures of Anthropogenic $CH_4$ Sources in Alberta, Canada, Atmos. Environ., 164, 280-288, https://doi.org/10.1016/j.atmosenv.2017.06.021, 2017.

Luther, A., Kleinschek, R., Scheidweiler, L., Defratyka, S., Stanisavljevic, M., Forstmaier, A., Dandocsi, A., Wolff, S., Dubravica, D., Wildmann, N., Kostinek, J., Jöckel, P., Nickl, A.-L., Klausner, T., Hase, F., Frey, M., Chen, J., Dietrich, F., Nęcki, J., Swolkień, J., Fix, A., Roiger, A., and Butz, A.: Quantifying $CH_4$ emissions from hard coal mines using mobile sun-viewing Fourier transform spectrometry, Atmos. Meas. Tech., 12, 5217-5230, https://doi.org/10.5194/amt-12-5217-2019, 2019.

Maazallahi, H., Fernandez, J. M., Menoud, M., Zavala-Araiza, D., Weller, Z. D., Schwietzke, S., von Fischer, J. C., Denier van der Gon, H., and Röckmann, T.: Methane mapping, emission quantification, and attribution in two European cities: Utrecht (NL) and Hamburg (DE), Atmos. Chem. Phys., 20, 14717-14740, https://doi.org/10.5194/acp-20-14717-2020, 2020.

Maazallahi, H., Delre, A., Scheutz, C., Fredenslund, A. M., Schwietzke, S., Denier van der Gon, H., and Röckmann, T.: Intercomparison of detection and quantification methods for methane emissions from the natural gas distribution network in Hamburg, Germany, Atmos. Meas. Tech., 16, 5051-5073, https://doi.org/10.5194/

https://doi.org/10.5194/egusphere-2024-2522
Preprint. Discussion started: 30 September 2024


amt-16-5051-2023, 2023.

Makarova, M. V., Alberti, C., Ionov, D. V., Hase, F., Foka, S. C., Blumenstock, T., Warneke, T., Virolainen, Y. A., Kostsov, V. S., Frey, M., Poberovskii, A. V., Timofeyev, Y. M., Paramonova, N. N., Volkova, K. A., Zaitsev, N. A., Biryukov, E. Y., Osipov, S. I., Makarov, B. K., Polyakov, A. V., Ivakhov, V. M., Imhasin, H. K., and Mikhailov, E. F.: Emission Monitoring Mobile Experiment (EMME): an overview and first results of the St. Petersburg megacity campaign 2019, Atmos. Meas. Tech., 14, 1047-1073, https://doi.org/10.5194/amt-14-1047-2021, 2021.

Masuda, S., Suzuki, S., Sano, I., Li, Y.-Y., and Nishimura, O.: The seasonal variation of emission of greenhouse gases from a full-scale sewage treatment plant, Chemosphere, 140, 167-173, https://doi.org/10.1016/j.chemosphere.2014.09.042, 2015.

Masuda, S., Sano, I., Hojo, T., Li, Y.-Y., and Nishimura, O.: The comparison of greenhouse gas emissions in sewage treatment plants with different treatment processes, Chemosphere, 193, 581-590, https://doi.org/10.1016/j.chemosphere.2017.11.018, 2017.

McKain, K., Down, A., Raciti, S. M., Budney, J., Hutyra, L. R., Floerchinger, C., Herndon, S. C., Nehrkorn, T., Zahniser, M. S., Jackson, R. B., Phillips, N., and Wofsy, S. C.: Methane emissions from natural gas infrastructure and use in the urban region of Boston, Massachusetts, Proc Natl Acad Sci USA, 112, 1941-1946, www.pnas.org/cgi/doi/10.1073/pnas.1416261112, 2015.

Moore, D. P., Li, N. P., Wendt, L. P., Castañeda, S. R., Falinski, M. M., Zhu, J.-J., Song, C., Ren, Z. J., and Zondlo, M. A.: Underestimation of Sector-Wide Methane Emissions from United States Wastewater Treatment, Environ. Sci. Technol., 57, 4082-4090, https://doi.org/10.1021/acs.est.2c05373, 2023.

Nassar, R., Hill, T. G., McLinden, C. A., Wunch, D., Jones, D. B. A., and Crisp, D.: Quantifying $CO_2$ emissions from Individual Power Plants From Space, Geophys. Res. Let.t, 44, 10045-10053, https://doi.org/10.1002/2017GL074702, 2017.

Picarro: Datasheet G2201-i $\delta^{13}C$ in $CH_4$ and $CO_2$ Gas Analyzer, available at:

https://doi.org/10.5194/egusphere-2024-2522
Preprint. Discussion started: 30 September 2024


https://www.picarro.com/environmental/support/library/documents/g2201i_analyzer_datasheet (last access: 5 August 2024), 2010.

Rella, C. W., Hoffnagle, J., He, Y., and Tajima, S.: Local- and regional-scale measurements of $CH_4$, $\delta^{13}CH_4$, and $C_2H_6$ in the Uintah Basin using a mobile stable isotope analyzer, Atmos. Meas. Tech., 8, 4539–4559, https://doi.org/10.5194/amt-8-4539-2015, 2015.

Richardson, S. J., Miles, N. L., Davis, K. J., Lauvaux, T., Martins, D. K., Turnbull, J. C., McKain, K., Sweeney, C., and Cambaliza, M. O. L.: Tower measurement network of in-situ $CO_2$, $CH_4$, and CO in support of the Indianapolis FLUX (INFLUX) Experiment. Elem. Sci. Anth., 5, 59, https://doi.org/10.1525/elementa.140, 2017.

Riddick, S. N., Connors, S., Robinson, A. D., Manning, A. J., Jones, P. S. D., Lowry, D., Nisbet, E., Skelton, R. L., Allen, G., Pitt, J., and Harris, N. R. P.: Estimating the size of a methane emission point source at different scales: from local to landscape, Atmos. Chem. Phys., 17, 7839-7851, https://doi.org/10.5194/acp-17-7839-2017, 2017.

Shi, T., Han, G., Ma, X., Mao, H., Chen, C., Han, Z., Pei, Z., Zhang, H., Li, S., and Gong, W.: Quantifying factory-scale $CO_2$/$CH_4$ emission based on mobile measurements and EMISSION-PARTITION model: cases in China, Environ. Res. Lett., 18, 034028, https://doi.org/10.1088/1748-9326/acbce7, 2023.

Song, C., Zhu, J.-J., Willis, J. L., Moore, D. P., Zondlo, M. A., and Ren, Z. J.: Methane emissions from municipal wastewater collection and treatment systems, Environ. Sci. Technol., 57, 2248-2261, https://doi.org/10.1021/acs.est.2c04388, 2023.

Stadler, C., Fusé, V. S., Linares, S., and Juliarena, P.: Estimation of methane emission from an urban wastewater treatment plant applying inverse Gaussian model, Environ. Monit. Assess., 194, 27, https://doi.org/10.1007/s10661-021-09660-4, 2021.

Sun, W., Deng, L., Wu, G., Wu, L., Han, P., Miao, Y., and Yao, B.: Atmospheric monitoring of methane in Beijing using a mobile observatory, Atmosphere, 10, 554, https://doi.org/10.3390/atmos10090554, 2019.

https://doi.org/10.5194/egusphere-2024-2522
Preprint. Discussion started: 30 September 2024


Sun, Y., Yang, T., Gui, H., Li, X., Wang, W., Duan, J., Mao, S., Yin, H., Zhou, B., Lang, J., Zhou, H., Liu, C., and Xie, P.: Atmospheric environment monitoring technology and equipment in China: A review and outlook, J. Environ. Sci., 123, 41-53, https://doi.org/10.1016/j.jes.2022.01.014, 2023.

Venkatram, A. and Horst, T. W.: Approximating dispersion from a finite line source, Atmos. Environ., 40, 2401-2408, https://doi.org/10.1016/j.atmosenv.2005.12.014, 2006.

Vítěz, T., Novák, D., Lochman, J., and Vítězová, M.: Methanogens diversity during anaerobic sewage sludge stabilization and the effect of temperature, Processes, 8, 822, https://doi.org/10.3390/pr8070822, 2020.

Vogel, F., Ars, S., Wunch, D., Lavoie, J., Gillespie, L., Maazallahi, H., Röckmann, T., Nęcki, J., Bartyzel, J., Jagoda, P., Lowry, D., France, J., Fernandez, J., Bakkaloglu, S., Fisher, R., Lanoiselle, M., Chen, H., Oudshoorn, M., Yver-Kwok, C., Defratyka, S., Morgui, J. A., Estruch, C., Curcoll, R., Grossi, C., Chen, J., Dietrich, F., Forstmaier, A., Denier van der Gon, H. A. C., Dellaert, S. N. C., Salo, J., Corbu, M., Iancu, S. S., Tudor, A. S., Scarlat, A. I., and Calcan, A.: Ground-Based Mobile Measurements to Track Urban Methane Emissions from Natural Gas in 12 Cities across Eight Countries, Environ. Sci. Technol., 58, 2271-2281, https://doi.org/10.1021/acs.est.3c03160, 2024.

von Fischer, J. C., Cooley, D., Chamberlain, S., Gaylord, A., Griebenow, C. J., Hamburg, S. P., Salo, J., Schumacher, R., Theobald, D., and Ham, J.: Rapid, Vehicle-Based Identification of Location and Magnitude of Urban Natural Gas Pipeline Leaks, Environ. Sci. Technol., 51, 4091-4099, https://doi.org/10.1021/acs.est.6b06095, 2017.

Wang, D., Ye, W., Wu, G., Li, R., Guan, Y., Zhang, W., Wang, J., Shan, Y., and Hubacek, K.: Greenhouse gas emissions from municipal wastewater treatment facilities in China from 2006 to 2019, Sci. Data., 9, 317, https://doi.org/10.1038/s41597-022-01439-7, 2022.

https://doi.org/10.5194/egusphere-2024-2522
Preprint. Discussion started: 30 September 2024


775 Wang, X., Wang, T., Chen, S., and Tang, Y.: Study on methane emission from
776 wastewater treatment plants-A case study of Wuhu city, Advances in Geosciences,
777 11, 677-689, https://doi.org/10.12677/AG.2021.115063, 2021.
778 Wang, Y., Tang, J., Li, F., Xie, D., Zuo, F., Yu, X., Xu, Y., and Chen, J.: Measurement
779 of methane emissions from CNG fueling stations in East China, Environ. Sci. Pollut.
780 R., 29, 71949-71957, https://doi.org/10.1007/s11356-022-20929-0, 2022a.
781 Wang, Y., Tang, J., Xie, D., Li, F., Xue, M., Zhao, B., Yu, X., and Wen, X.: Temporal
782 variation and grade categorization of methane emission from LNG fueling stations,
783 Sci. Rep., 12, 18428, https://doi.org/10.1038/s41598-022-23334-2, 2022b.
784 WMO：WMO greenhouse gas Bulletin. The state of greenhouse gases in the atmosphere
785 based on global observations through 2022. https://library.wmo.int/idurl/4/68532,
786 2023.
787 Yacovitch, T. I., Herndon, S. C., Petron, G., Kofler, J., Lyon, D., Zahniser, M. S., and
788 Kolb, C. E.: Mobile Laboratory Observations of Methane Emissions in the Barnett
789 Shale Region, Environ. Sci. Technol., 49, 7889-7895, https://doi.org/10.1021/
790 es506352j, 2015.
791 Yin, Y., Qi, X., Gao, L., Lu, X., Yang, X., Xiao, K., Liu, Y., Qiu, Y., Huang, X and Liang,
792 P.: Quantifying methane influx from sewer into wastewater treatment processes,
793 Environ. Sci. Technol., 58, 9582-9590, https://doi.org/10.1021/acs.est.4c00820,
794 2024.
795 Zhang, Y., Jacob, D. J., Lu, X., Maasakkers, J. D., Scarpelli, T. R., Sheng, J.-X., Shen,
796 L., Qu, Z., Sulprizio, M. P., Chang, J., Bloom, A. A., Ma, S., Worden, J., Parker, R.
797 J., and Boesch, H.: Attribution of the accelerating increase in atmospheric methane
798 during 2010–2018 by inverse analysis of GOSAT observations, Atmos. Chem. Phys.,
799 21, 3643–3666, https://doi.org/10.5194/acp-21-3643-2021, 2021.
800 Zhao, T., Yang, D., Liu, Y., Cai, Z., Yao, L., Che, K., Ren, X., Bi, Y., Yi, Y., Wang, J.,
801 and Zhu, S.: Development of an Integrated Lightweight Multi-Rotor UAV Payload
802 for Atmospheric Carbon Dioxide Mole Fraction Measurements, Atmosphere, 13, 855,

https://doi.org/10.5194/egusphere-2024-2522
Preprint. Discussion started: 30 September 2024


https://doi.org/10.3390/atmos13060855, 2022.

Zhao, Y., Xue, M., Li, X., Liu, G., Liu, S., and Sun, X.: Application of Vehicle-Mounted Methane Detection Method in the Oil and Gas Industry, Environmental Protection of Oil & Gas Fields, 31, 4, https://doi.org/10.3969/j.issn.1005-3158.2021.04.001, 2021.

Zimnoch, M., Necki, J., Chmura, L., Jasek, A., Jelen, D., Galkowski, M., Kuc, T., Gorczyca, Z., Bartyzel, J., and Rozanski, K.: Quantification of carbon dioxide and methane emissions in urban areas: source apportionment based on atmospheric observations, Mitig. Adapt. Strateg. Glob. Change, 24, 1051-1071, https://doi.org/10.1007/s11027-018-9821-0, 2018.